



Understanding the causes of rapidly declining prediction skill of the East Asian summer monsoon rainfall with lead time in BCC_CSM1.1m

Na Wang^{1,3} · Hong-Li Ren² · Yi Deng³ · Siyu Zhao⁴

Received: 21 November 2020 / Accepted: 17 May 2021 / Published online: 27 June 2021
© The Author(s), under exclusive licence to Springer-Verlag GmbH Germany, part of Springer Nature 2021

Abstract

Dynamical prediction of monsoon rainfall has been an important topic and a long-standing issue in both research and operational community. This paper provides a comprehensive evaluation of the subseasonal-to-seasonal (S2S) prediction skill of the East Asian summer monsoon (EASM) rainfall using the hindcast record from the Beijing Climate Center Climate System Model, BCC CSM1.1m, during the period 1983–2019. The model exhibits reasonable skills for predicting the EASM rainfall at all lead times with the skill dropping dramatically from the shortest lead time of about 2 weeks (LM0) to 1-month lead (LM1), and then fluctuating remarkably throughout 2-month to 12-month lead times. Over the EASM domain, the rapid decline of the S2S rainfall prediction skill from LM0 to LM1 is mainly caused by the inferior skills over Central China in July and over Northeast China in August. Composite analysis based on hindcast records suggest that these inferior skills are directly tied to the model's difficulties in capturing above-normal precipitation over eastern Central China and Northeast China in the respective months, which are further shown to be associated with anomalous weakening and meridional movement of the Northwestern Pacific subtropical high and the activity of large-scale teleconnection pattern hard to be predicted over northeastern Asia in summer, respectively. These findings inform the intrinsic limits of the S2S predictability of the EASM rainfall by a dynamical model, and strongly suggest that the level of confidence placed upon S2S forecasts should be stratified by large-scale circulation anomalies known to significantly affect the prediction skill, e.g., the subtropical high and high-latitude teleconnection patterns for summer monsoon rainfall prediction in this region.

Keywords East Asian monsoon · Subseasonal-to-seasonal prediction · Lead time · BCC_CSM1.1m

1 Introduction

The East Asian monsoon features a distinct annual reversal of surface winds and the associated rainy summer and dry winter (Ramage 1971; Trenberth et al. 2000). Because of the Tibetan-Iranian Plateau, the strong anthropogenic forcing from aerosol emissions and the intricate teleconnection with adjacent ocean basins, etc., the East Asian monsoon has its own characteristics including the onset, S2S evolution and variability across longer timescales (Tzeng and Lee 2001; Liu et al. 2018; Dong et al. 2019; Li et al. 2019; Son et al. 2019). Additionally, the East Asian summer monsoon (EASM) rainfall is the life blood of over one-fifth of the world's population, and also plays an essential role in regulating regional atmospheric circulation and hydrological cycle. Since the variabilities of summer monsoon rainfall impose major impacts on the occurrence probability of natural disasters (e.g., floods and droughts), agricultural

✉ Hong-Li Ren
renhl@cma.gov.cn

✉ Yi Deng
yi.deng@eas.gatech.edu

¹ Shandong Climate Center, Meteorology Bureau of Shandong Province, Jinan 250031, China

² State Key Laboratory of Severe Weather, Chinese Academy of Meteorological Sciences, 46 Zhongguancun, Haidian District, Beijing 100081, China

³ School of Earth and Atmospheric Sciences, Georgia Institute of Technology, 311 Ferst Drive, Atlanta, GA 30332-0340, USA

⁴ Department of Atmospheric and Oceanic Sciences, University of California, Los Angeles, CA 90095, USA

productivity and water resources in East Asia, the enhanced accuracy of predicting the EASM rainfall and the tailored operational application are of great scientific and socioeconomic significance.

During the past several decades, substantial efforts have been devoted to improving seasonal prediction skill of dynamical models. In comparison to the incipient atmospheric models (Charney and Shukla 1981; Shukla 1998), the current state-of-the-art coupled atmosphere–ocean–land–cryosphere models exhibit considerable enhancement of the forecast performance for monsoon regions, and have gradually become an indispensable tool of summer monsoon rainfall prediction (Kug et al. 2008; Ma and Wang 2014; Park et al. 2018). In 2013, the World Weather Research Program (WWRP) and the World Climate Research Program (WCRP) jointly established the Subseasonal-to-Seasonal (S2S) prediction project to bridge the gap between medium-to-long range weather forecast and seasonal climate prediction, and to deepen the understanding of the sources of S2S predictability and bring together the weather and climate research communities to improve forecast skill on the timescales of particular relevance to the Global Framework for Climate Services (GFCS) (Vitart and Robertson 2018; de Andrade et al. 2019; Wang et al. 2020c). At present, the studies of annual variability of summer monsoon and intraseasonal process of monsoon system are conducted in parallel and complement each other, bringing about the new challenge and opportunity for the dynamical prediction of the EASM rainfall (Jie et al. 2017; Li et al. 2020; Son et al. 2020; Zhou et al. 2020).

The world's key climate research and operational institutions now provide real-time predictions by the latest models covering subseasonal-to-interannual time ranges as well as the related retrospective records. For instance, the 9-month, 7-month and 13-month lead time predictions of climate variables, important phenomena and predominant modes are produced by the CFSv2 model at the National Centers for Environmental Prediction (NCEP; Saha et al. 2014), by the SEAS5 model at the European Centre for Medium-range Weather Forecasts (ECMWF; Johnson et al. 2019) and by the BCC_CSM1.1m model at the Chinese National Climate Center (NCC; Wu et al. 2014). Middle-to-high level skilled predictions for 2-m temperature, precipitation, monsoon systems, and El Niño–Southern Oscillation, etc., made by these models have been reported in many studies (e.g., Liu et al. 2015, 2021; Liu and Ren 2015, 2017; Park et al. 2018; Keane et al. 2019; Wang et al. 2020b).

Due to the large uncertainty of climate models, derived from the imperfect representations of diverse physical processes (e.g., cloud microphysics, momentum and energy transport between stratosphere and troposphere, etc.) and forcings (e.g., aerosol, land-use, volcano, etc.), dynamical prediction of summer monsoon rainfall variability remains

a challenging task. Higher prediction skills of precipitation and circulation are mostly found over the equatorial central-eastern Pacific and tropical regions, respectively, while the performance is much less satisfying over monsoon domains and extratropical regions, even at the shortest lead time (Liu et al. 2015; Singh et al. 2019). In terms of BCC_CSM1.1m, its S2S prediction skill of the EASM rainfall has yet to be systematically examined. In this study, efforts are made to address the following specific questions: (1) How does the model's performance in the EASM rainfall prediction vary across different lead times? (2) What limits the subseasonal rainfall predictability over the EASM domain? (3) What processes are responsible for the rapid drop of prediction skill with the increase of lead time?

The remainder of this paper is organized as follows. Model, datasets and analysis methods used are described in Sect. 2. Predictability evaluation of the EASM rainfall is reported in Sect. 3. In Sect. 4, we demonstrate how the skill of subseasonal rainfall prediction varies according to the large-scale circulation anomalies present over the EASM domain. Summary and additional discussion are provided in Sect. 5.

2 Model, data and methodology

2.1 Model, hindcast and observational data

The upgraded version of the Beijing Climate Center Climate System Model version 1.1 with a moderate atmospheric resolution (BCC_CSM1.1m; Wu et al. 2014) is assessed. The atmospheric component in this coupled model is BCC_AGCM2.2 with a horizontal resolution of T106, approximately $1^\circ \times 1^\circ$ in longitude and latitude, and 26 hybrid sigma/pressure levels in the vertical direction (Wu et al. 2010). The ocean and sea-ice components are the Geophysical Fluid Dynamics Laboratory (GFDL) Modular Ocean Model version 4 and the GFDL Sea Ice Simulator, respectively, with a tripolar grid $1^\circ \times 0.33^\circ$ in the horizontal direction and 40 vertical levels (Winton 2000; Griffies et al. 2005). The land model is the BCC Atmosphere and Vegetation Interaction Model version 1.0 with the same horizontal resolution as the atmospheric component (Ji et al. 2008). The different components are coupled without any flux correction.

The model hindcasts cover the period 1983–2014, initiated on the first day of each calendar month with 13-month forecast outputs that include the initial month and the next 12 months covering subseasonal–seasonal–annual timescales. The real-time forecast using this model was started in 2015. The atmospheric initial values are initialized from the four-time daily NCEP/NCAR Reanalysis 1, and those of the oceans are from the ocean temperature of the Global Oceanic

Data Assimilation System, through a nudging scheme with a relaxation timescale of 2 days. The BCC_CSM1.1m ensemble system includes nine empirical singular vector scheme members (Cheng et al. 2010) and 15 lagged average forecast scheme members of which the atmospheric and oceanic initial conditions on 5 days and 3 days preceding the first day of each month are combined to generate 15 perturbations (Ren et al. 2017). The 24 members of each variable are used to obtain the ensemble mean used for evaluating the model's prediction performance in this study.

Observational product of precipitation used for model assessment is the monthly precipitation from the Global Precipitation Climatology Project version 2.3 (GPCP; Adler et al. 2018) provided by the NOAA Physical Sciences Laboratory (<https://psl.noaa.gov/data/gridded/data.gpcp.html>). The circulation and sea surface temperature datasets are the fifth generation of the ECMWF atmospheric reanalyses (ERA5; Hersbach et al. 2020) obtained from the Climate Data Store (<https://cds.climate.copernicus.eu/cdsapp#!/search?type=dataset>).

Both model and observational datasets cover the period from January 1983 to December 2019. Summer refers to June–July–August (JJA) in the Northern Hemisphere (NH) and December–January–February (DJF) in the Southern Hemisphere (SH), and winter refers to DJF in NH and JJA in SH, respectively. For the model's 13-month forecast outputs, the runs at the first time (i.e., the prediction for the initial month) are extracted monthly between 1983 and 2019 and combined as the 0-month lead (LM0) forecasts; the data at the second time (i.e., the prediction for the month following the initial month) are extracted monthly and combined as the 1-month lead (LM1) forecasts; and so forth until the outputs at the thirteenth month are extracted and recombined as the 12-month lead (LM12) forecasts. It is worth noting that at a given lead, e.g., LM0, the initial months for summer rainfall and those for monthly rainfall in June, July, and August are different. Considering the systematic error, the model climatology is calculated at each lead time and is a function of the initial calendar and lead month.

2.2 Metrics of prediction skill evaluation

Predictability of the EASM rainfall is evaluated with two skill metrics recommended by the World Meteorological Organization: the temporal correlation coefficient (TCC, Eq. 1), representing the predictability of each spatial grid so that we could obtain a spatial distribution of prediction skill; the spatial correlation coefficient (SCC, Eq. 2), measuring the level of spatial pattern similarity between prediction and observation.

Define $x_{i,j}$ and $p_{i,j}$ as the anomalies for observation and prediction in space (i) and time (j); M is the number of space samples and N is the number of time samples.

The TCC is calculated as

$$TCC_i = \frac{\sum_{j=1}^N (x_{i,j} - \bar{x}_i) \times (p_{i,j} - \bar{p}_i)}{\sqrt{\sum_{j=1}^N (x_{i,j} - \bar{x}_i)^2} \times \sqrt{\sum_{j=1}^N (p_{i,j} - \bar{p}_i)^2}} \quad (1)$$

where $\bar{x}_i = \frac{1}{N} \sum_{j=1}^N x_{i,j}$, $\bar{p}_i = \frac{1}{N} \sum_{j=1}^N p_{i,j}$.

The SCC is calculated as

$$SCC_j = \frac{\sum_{i=1}^M (x_{i,j} - \bar{x}_j) \times (p_{i,j} - \bar{p}_j)}{\sqrt{\sum_{i=1}^M (x_{i,j} - \bar{x}_j)^2} \times \sqrt{\sum_{i=1}^M (p_{i,j} - \bar{p}_j)^2}} \quad (2)$$

where $\bar{x}_j = \frac{1}{M} \sum_{i=1}^M x_{i,j}$, $\bar{p}_j = \frac{1}{M} \sum_{i=1}^M p_{i,j}$.

The range of the TCC and SCC are from -1.0 to 1.0 , and a large positive (negative) value indicates a highly similar (opposite) correlation between prediction and observation.

2.3 Definition of the East Asian summer monsoon domain

The definition of monsoon domains evolved during the past hundreds of years of research. Traditionally, the monsoon region is delineated by surface winds (Ramage 1971). Further refinements of the definition of monsoon climate considered the reversal of wind direction, the features of divergence fields and vertical air movements (Wang et al. 2008). Li and Zeng (2002, 2003) introduced a unified dynamical index of monsoon, the dynamical normalized seasonality, to study the issue of monsoons. All of the tropical, subtropical, and temperate-frigid monsoons over the EASM domain are shown by this definition. Considering the essential role of monsoon rainfall relate latent heating and key parameters in hydrological cycle also led to the modern definition of monsoon domain emphasizing precipitation characteristics. Here, we adopt the objective definition for the global monsoon precipitation domain by the annual range and the annual precipitation (Wang and Ding 2006) to identify the EASM domain. The annual range is defined by the local summer-minus-winter precipitation and used to measure monsoon precipitation intensity. The EASM domain is defined by the land region in which the annual range exceeds 180 mm and the local summer precipitation exceeds 35% of the annual precipitation. This definition is in excellent agreement with the monsoon domain of Li and Zeng (2005), and previously defined through more complex criteria (Wang and Ho 2002).

Overall, BCC_CSM1.1m realistically reproduces the global climatologies of the annual range and the annual precipitation from 0 to 12-month lead times as their correlation coefficients (CCs) with observations are from 0.72 to 0.76 for the annual range and are from 0.86 to 0.92 for the annual precipitation, which is critical for the further definition of monsoon domains in the model. As shown in

Fig. 1, the Asian monsoon domain is effectively captured by LM0. However, overestimated annual range (Fig. 1a, b) and annual precipitation (Fig. 1c, d) are showed over the tropical Northwest Pacific, causing an eastward stretch of the Asian monsoon domain to the central North Pacific. Here, we set the longitude of 95° E as the western boundary of the EASM domain which is slightly narrowed and more northward extended in the model compared with the observation. These biases are found across multiple lead times. Kim et al. (2012) and Kitoh et al. (2013) discussed similar biases in the hindcasts of the ECMWF System 4 and NCEP CFSv2 and the simulations from the CIMAP5 models, suggesting potential intrinsic limits in these dynamical models.

3 Prediction skill assessment for the East Asian summer monsoon rainfall

CCs for the climatologies of summer rainfall between the prediction at each lead month and the GPCP observation have values ranging from 0.76 to 0.78 over the EASM domain. The model captures the general distribution of summer rainfall but tends to overestimate the rainfall over the tropical Northwest Pacific and underestimate the rainfall over the EASM domain (Fig. 2a, b). Similar biases also exist in the ECMWF System 4, NCEP CFSv2 and CIMAP6 models (Kim et al. 2012; Wang et al. 2020a).

The prediction skill of EASM rainfall is measured by TCC between model rainfall hindcasts and observation. Prediction at LM0 shows considerable skill over most monsoon domain except rarely negative values (Fig. 2c). While at LM1, the unskillful areas occupy the northeast China and the sparse central and southern Asia (Fig. 2d), and expand

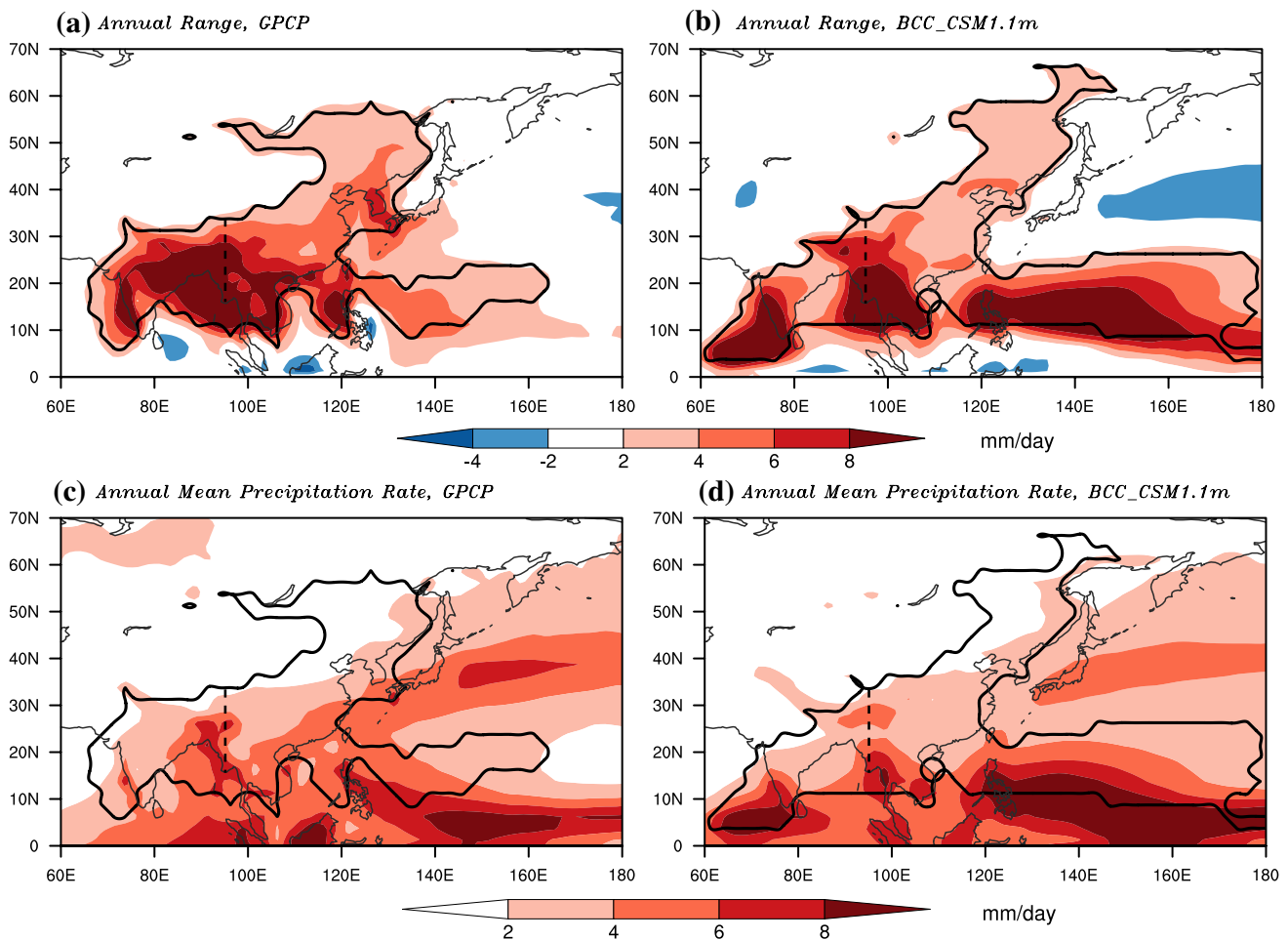


Fig. 1 The climatological mean for the annual range of precipitation (a, b) and the annual mean precipitation rate (c, d). The bold lines delineate the Asian monsoon domain and the dashed lines delineate

the western boundary of the East Asian summer monsoon domain. a, c Observation and b, d 0-month lead of model

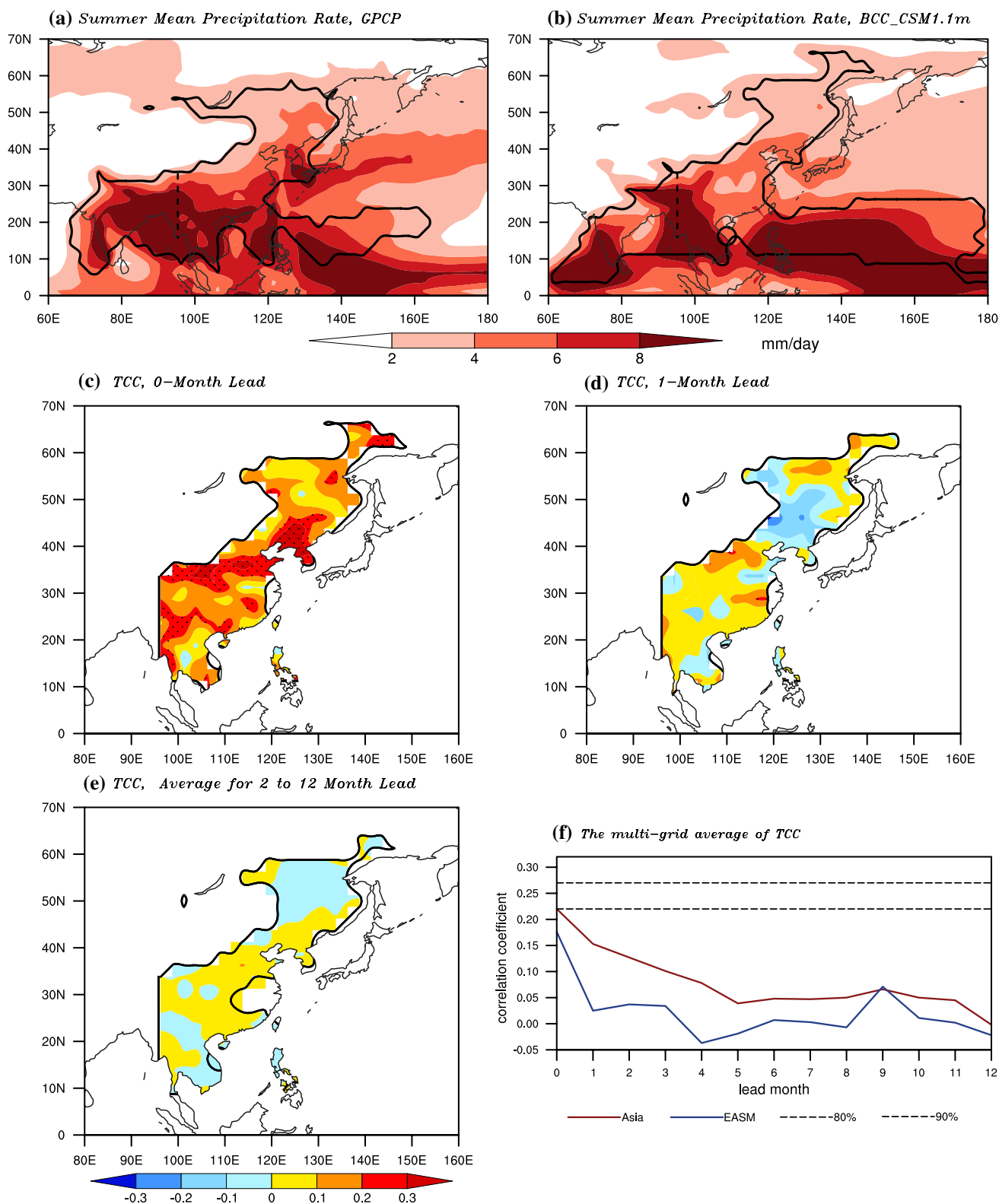


Fig. 2 a, b Same as Fig. 1. a, b But for the summer mean precipitation rate. Spatial distribution of temporal correlation coefficients (TCCs) for summer rainfall over the East Asian summer monsoon domain based on the observation and the model outputs at 0-month lead (LM0) (c), 1-month lead (d) and averaged 2-month to 12-month

lead (LM12) (e); stipple areas represent the statistical significance at the 0.2 level. f The regionally averaged TCCs for summer rainfall at LM0 to LM12 over the Asian (red line) and the East Asian (blue line) monsoon domain; the two gray dashed lines represent the statistical significance at the 0.1 and 0.2 levels

further at longer lead times (Fig. 2e). We display the averaged results of LM2-12 here, given that long-lead predictions become more similar to each other due to the dominant role played by the slowly varying components in the model. The regionally averaged TCCs over the Asian and the EASM monsoon domain at 0 to 12-month lead times are calculated and plotted in Fig. 2f. Generally speaking, skills decrease gradually throughout LM0 to LM5 and remain nearly flat at longer lead times over the Asian monsoon domain and the skills drop rapidly from LM0 to LM1 with remarkable fluctuations throughout LM2 to LM12 over the EASM domain.

The EASM rainfall prediction is characterized by a rapid deterioration of skill from LM0 to LM1 in BCC_CSM1.1m, demanding a more detailed examination of factors affecting such skills across subseasonal timescales. Figure 3 shows the model's prediction skills of monthly rainfall in June, July and August over the EASM domain. At LM0 (Fig. 3a, d, g), the significantly skillful areas are located over the southern Asia in June, central China in July and eastern China in August, respectively. Prediction performance for these three months commonly suffer from reduced skill and expanded unskillful areas throughout LM1 to LM12 (Fig. 3b, c, e, f,

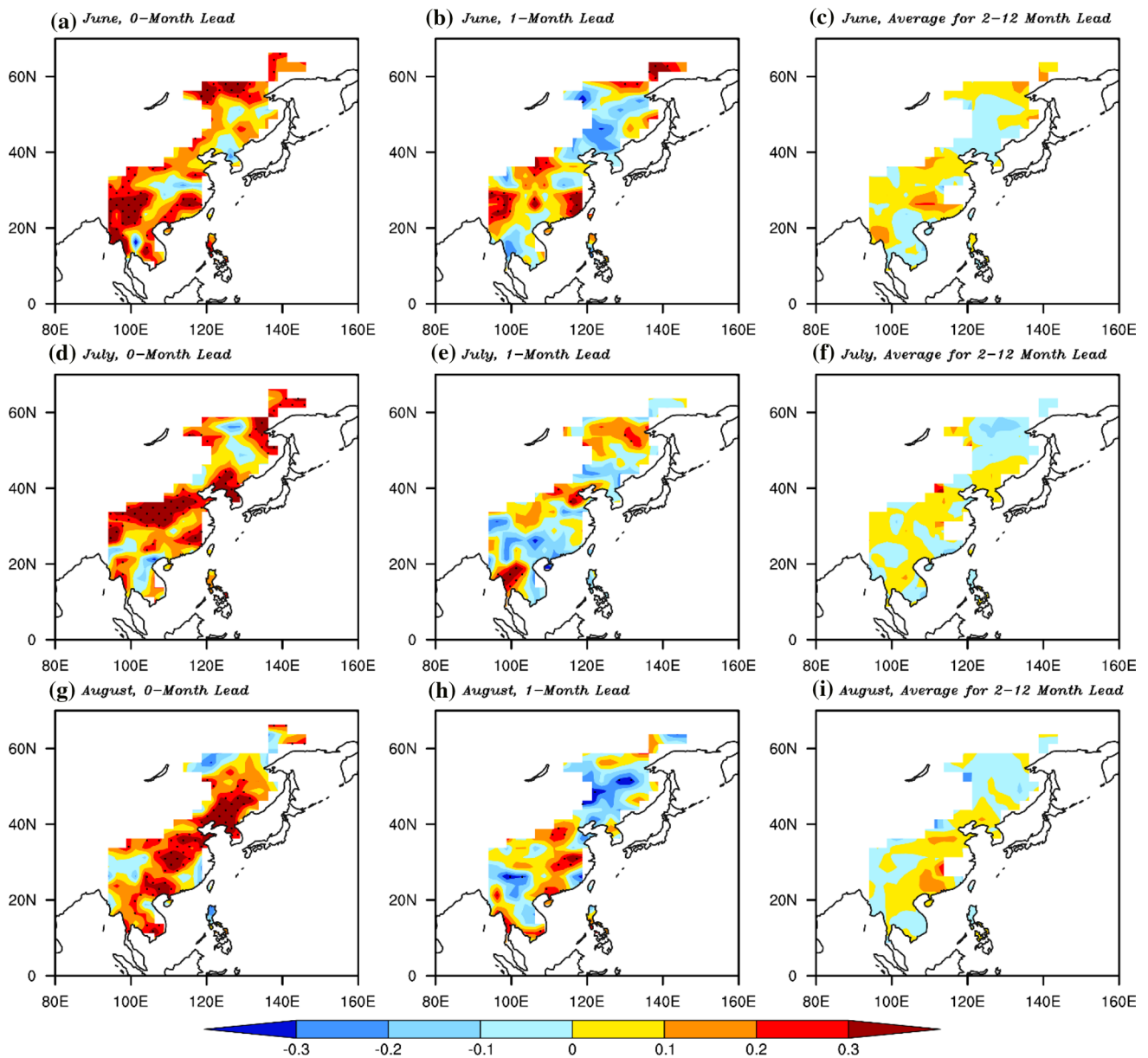


Fig. 3 Spatial distribution of temporal correlation coefficients for monthly rainfall over the East Asian summer monsoon domain between the observation and the model outputs at 0-month lead (**a, d,**

g), 1-month lead (**b, e, h**) and averaged 2-month to 12-month lead (**c, f, i**) in June (**a, b, c**), July (**d, e, f**) and August (**g, h, i**); stipple areas represent the statistical significance at the 0.2 level

h, i). The major differences in the unskillful areas at LM1 compared to LM0 are situated over Northeast China in June and August, and over South China in July.

The regionally averaged TCCs drop dramatically from LM0 to LM1, especially in July and August, and gradually decrease or fluctuate at LM2 to LM12 (Fig. 4i). The differences in the TCC between LM1 and LM0 clearly mark regions of rapid declining skills: most notably over Northeast China throughout all LM1 to LM12 (Fig. 4a, e) and two smaller areas over Central China and from Southwest China to Southeast Asia. More specifically, the inferior skills over Central China in July (Fig. 4c, g) and over Northeast China in August (Fig. 4d, h) account for majority of the degradation of the S2S prediction skill over the EASM domain. For rainfall in June (Fig. 4b, f), the prediction skill also rapidly drops at LM1 over Northeast China, but not as pronounced as that for rainfall in August.

4 Identification of factors affecting skills of subseasonal rainfall prediction over the East Asian summer monsoon domain

We now confirm that the reduced skill of EASM rainfall prediction at LM1 is largely associated with the drop of skills over Central China in July and over Northeast China in August. These two locations are marked in Fig. 5a. Regionally averaged TCCs in each month of summer indicate that the predictions are most skillful in July over Central China (Fig. 5b) and in August over Northeast China (Fig. 5c) at LM0, but become much less skillful at LM1.

SCC is employed to further examine the predictions skills over these two regions at LM0 and LM1 (Fig. 5d, e). The multi-year averaged SCCs at LM0 and LM1 are 0.14 and 0.02 over Central China in July, and 0.35 and 0.27 over

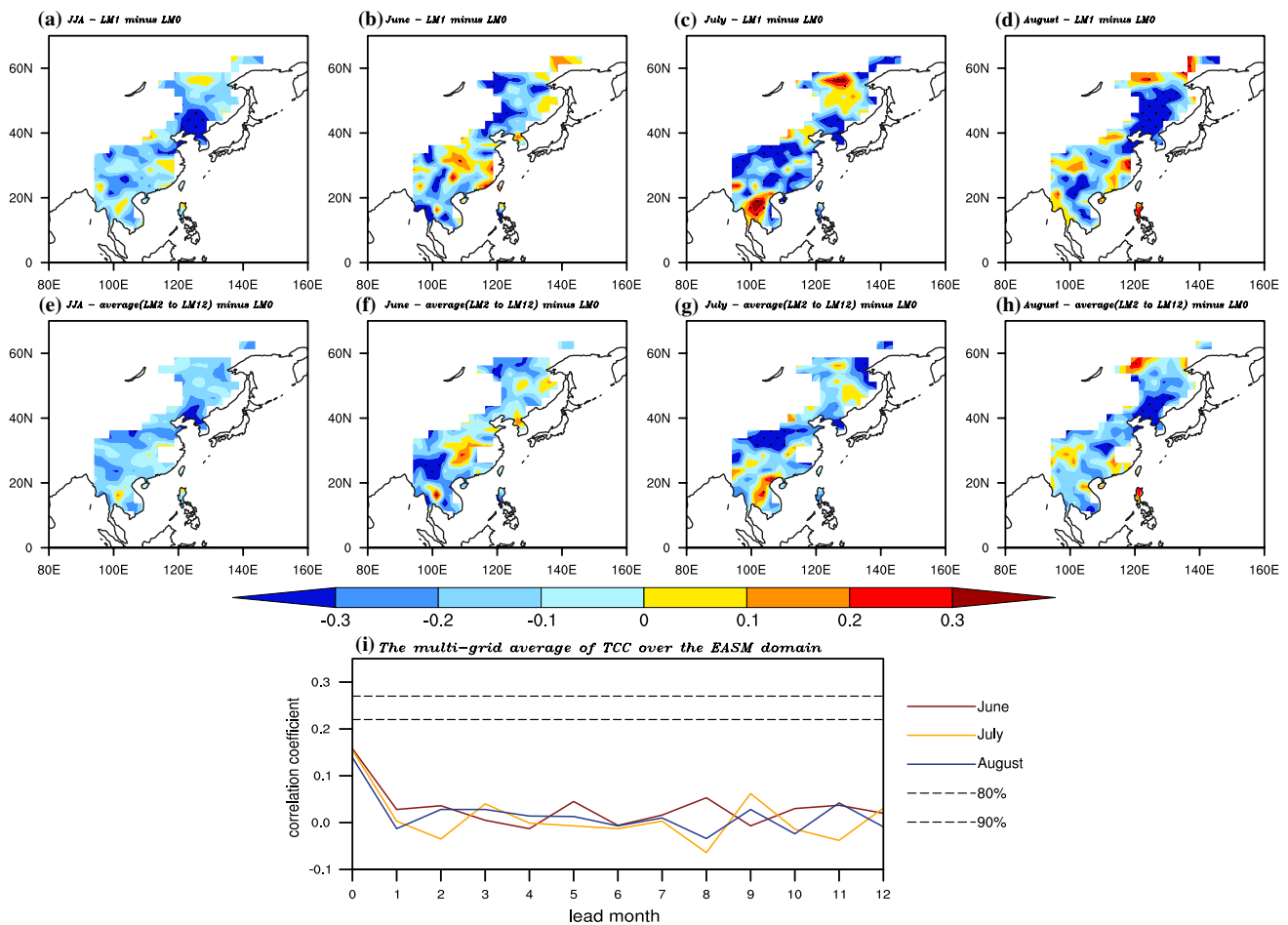


Fig. 4 Spatial distribution of the difference of temporal correlation coefficient (TCC) at 1-month lead minus that of 0-month lead (LM0) (a–d), and averaged 2-month to 12-month lead (LM12) minus that of 0-month lead (e–h) in summer (a, e), June (b, f), July (c, g) and August (d, h); stipple areas represent the statistical significance at

the 0.2 level. **i** The regionally averaged TCCs for June (red line), July (yellow line) and August (blue line) rainfall at LM0 to LM12 over Asian land monsoon domain; the two gray dashed lines represent the statistical significance at the 0.1 and 0.2 levels

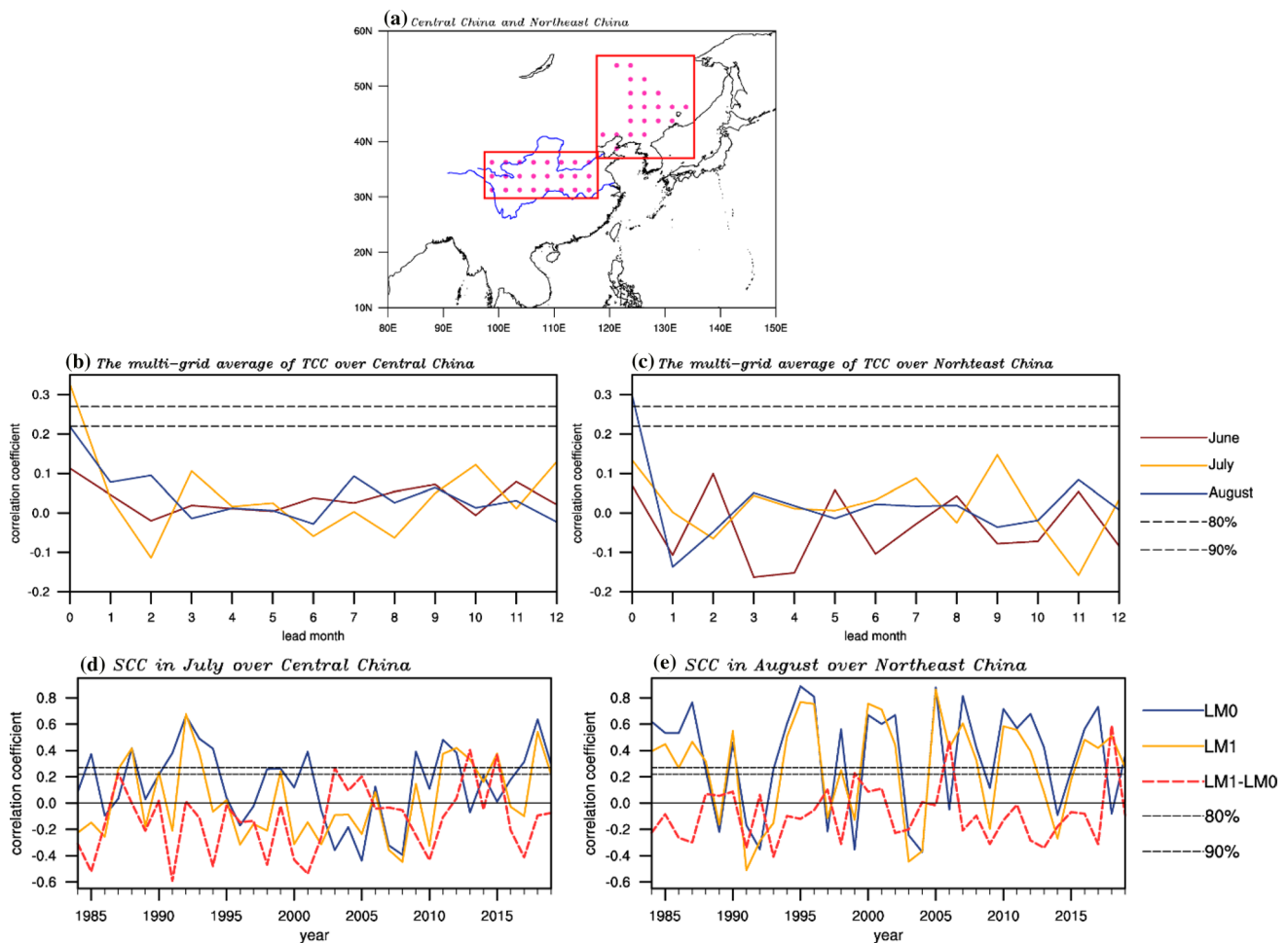


Fig. 5 **a** Locations of Central China and Northeast China (red rectangles) and the grids of GPCP data inside of them (purple stipples); two blue curve lines represent the Yangtze River and the Yellow River. The regionally averaged temporal correlation coefficients for June (red line), July (yellow line) and August (blue line) rainfall at 0 to 12-month lead times over Central China (**b**) and Northeast China (**c**),

respectively. The time series of spatial correlation coefficients for rainfall over Central China in July (**d**) and Northeast China in August (**e**) at 0-month lead (LM0) (blue line) and 1-month lead (LM1) (yellow line), and the differences of those at LM1 minus those at LM0 (red dashed line). The gray dashed lines represent the statistical significance at the 0.1 and 0.2 levels

Northeast China in August, respectively. Compared with LM0, there are 27 years and 25 years when the SCCs at LM1 are smaller over Central China and over Northeast China, respectively. The time series of SCC are characterized by pronounced interannual variations, suggesting substantial year-to-year variability in the subseasonal prediction skills over these two regions. We take advantage of this interannual variability to identify and understand what factors might contribute to the rapid decline of prediction skill from LM0 to LM1. Specifically, we separate the record (LM0–LM1) into reduced skill years and comparable skill years based on the differences of SCC between LM1 and LM0 in each year. For both Central China and Northeast China, the respective 8 years with SCCs at LM0 greater than 0.1 and with the largest absolute values of SCC differences (LM1 – LM0) are defined as the reduced skill years; the

respective 8 years with SCCs at LM0 and LM1 both greater than 0.1 and the smallest absolute value of SCC differences (LM1 – LM0) are defined as the comparable skill years. Here, we set one of the criteria as the SCC equals 0.1, which is not considered statistically significant. However, this will not be a major factor in our analysis given (1) the well-known low predictive skill of rainfall for East Asia in warm season, (2) the sensitivity of the correlations to the choice of the analysis domain, and (3) most importantly, the fact that these correlation coefficients are used only to classify forecasts into groups of “reduced skill” and “comparable skill” over two different forecast lead times with the absolute values of “skill/correlation” being of secondary importance. The 8 years in each group for Central China (Table 1) and for Northeast China (Table 2) are identified and used in the composite analysis that follows.

Table 1 Composite reduced skill years and comparable skill years based on the differences of the spatial correlation coefficients of the rainfall anomaly over Central China in July between 1-month lead and 0-month lead of the BCC_CSM1.1m, as well as the corresponding differences

Reduced skill		Comparable skill	
Difference (LM1 – LM0)	Year	Difference (LM1 – LM0)	Year
- 0.59	1991	- 0.05	2014
- 0.54	2001	- 0.04	2006
- 0.52	1985	- 0.02	1999
- 0.48	1994	- 0.02	1995
- 0.47	1998	0.00	1988
- 0.43	2010	0.01	1992
- 0.43	2000	0.02	1990
- 0.41	2017	0.04	2012

Table 2 Same as Table 1 but over Northeast China in August

Reduced skill		Comparable skill	
Difference (LM1 – LM0)	Year	Difference (LM1 – LM0)	Year
- 0.41	1993	- 0.08	2016
- 0.34	2013	- 0.07	2015
- 0.31	2017	- 0.06	1996
- 0.31	2009	- 0.02	2005
- 0.31	1998	- 0.01	2011
- 0.30	1987	0.07	1988
- 0.28	2012	0.09	2000
- 0.26	1986	0.09	1990

4.1 Central China

The composite pattern of the observed rainfall anomaly over Central China in July is characterized by above-normal

(below-normal) rainfall over the eastern (western) portion of the region in reduced skill years (Fig. 6a), meaning the prediction of the rainfall in July over eastern Central China is more skillful at LM0 than that at LM1. This pattern is reversed in comparable skill years and the model exhibits the capability to predict the rainfall over western Central China at both LM0 and LM1 (Fig. 6b). In other words, BCC_CSM1.1m shows higher capability to forecast rainfall in July over western Central China compared to that over eastern Central China.

Figure 7 shows the counterpart composites of the July 500-hPa geopotential height and 850-hPa vector wind based on the ERA5 reanalysis and the BCC_CSM1.1 outputs. According to the ERA5 (Fig. 7a–c), the rainfall distribution over Central China are largely modulated by the intensity and location of the Northwestern Pacific subtropical high (NWPSH) (southeasterly winds along the southern edge of NWPSH) and westerly winds over South China Sea in lower troposphere. Compared with the comparable skill years, the observed NWPSH appears less intense and displaced slightly northward and westward in reduced skill years. Additionally, a positive geopotential height anomaly is seen over the Yellow Sea at about 40° N, facilitating the northward transport of moisture from the southern ocean to the east part of Central China.

In the reduced skill years, the model shows reasonable skill in predicting the intensity and location anomalies of the NWPSH and the positive geopotential height anomaly around 40° N, 120° E at LM0 (Fig. 7d). While at LM1, the model has difficulty in reproducing the NWPSH anomaly realistically, and the intensity of the positive geopotential height anomaly over the Yellow Sea is much weaker (Fig. 7g). In the comparable skill years, the model fails to predict the westward movement of the NWPSH at both LM0 (Fig. 7e) and LM1 (Fig. 7h) but captures the negative geopotential height anomaly north of the NWPSH, restricting northward movement of the NWPSH. Besides, one

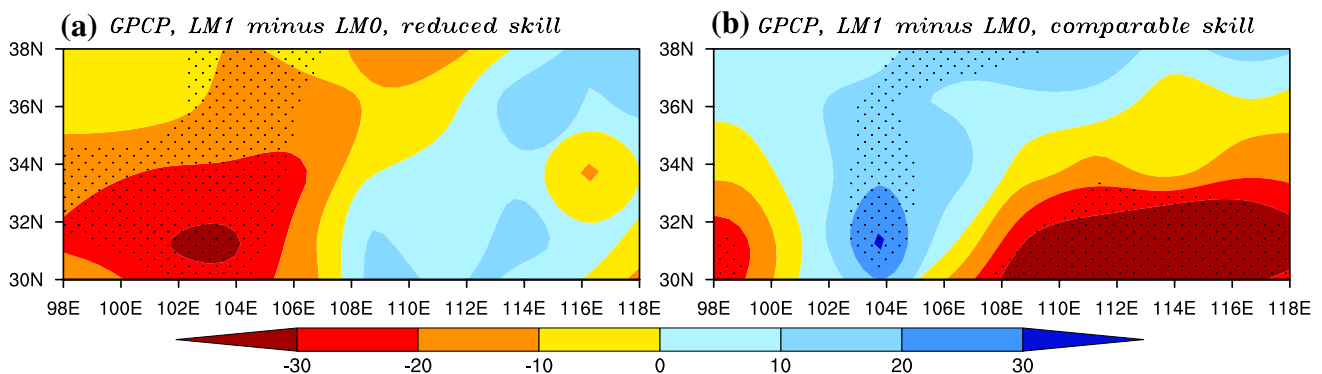


Fig. 6 Observational composite patterns of rainfall anomaly (mm) based on the reduced (a) and comparable (b) skilled years over Central China in July; stipple areas represent the statistical significance at the 0.2 level

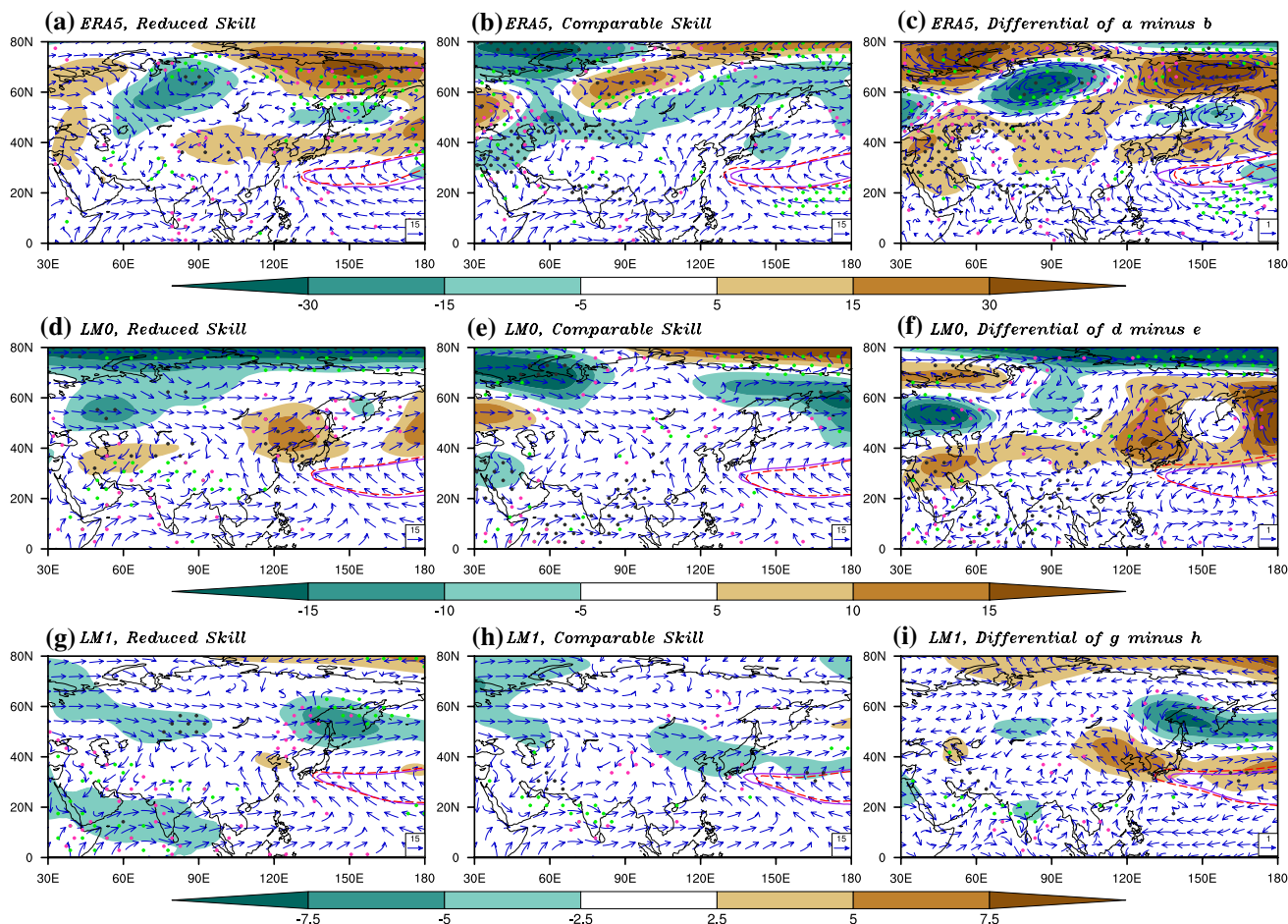


Fig. 7 Composite and difference patterns of 500-hPa geopotential height anomaly (gpm) and the 850-hPa vector wind (m s^{-1}), corresponding with Central China. **a–c** ERA5 reanalysis, **d–f** 0-month lead and **g–i** 1-month lead of model. Shades represent the geopotential height anomaly; vectors represent composite wind (**a, b, d, e, g, h**)

and differences of anomalous wind (**c, f, i**); purple solid lines and red dashes represent the climatology and composite 5880 gpm of observation and 5760 gpm of model; black, green and red dots represent the statistical significance at the 0.2 level for geopotential height, eastward and northward component of wind, respectively

distinction about the NWPSH is the much weaker intensity in the reduced skill years than that in the comparable skill years (Fig. 7c). Although the model could not reproduce it accurately at LM0 (Fig. 7f), we can see that in contrast to the observation, the model forecasts a stronger NWPSH at LM1 in the reduced skill years (Fig. 7i). Liu et al. (2014) and de Andrade et al. (2019) also found that in CFSv2 and S2S models, the middle-to-high latitudes circulation hind-cast quality, including that of the NWPSH, is low after the second week of lead time, likely due to the inherent unpredictability of the extratropical variability and the resulted errors in representing teleconnections.

4.2 Northeast China

The observed August rainfall over Northeast China is above-normal in reduced skill years (Fig. 8a) and below-normal in comparable skill years (Fig. 8b). This indicates that the

model shows reasonable skills in less rainfall prediction at both LM0 and LM1, but performs higher skills in predicting above-normal rainfall at LM0 than those at LM1. In other words, the model is more difficult in predicting rainfall in this region across subseasonal timescales.

The counterpart observed circulation composites show the establishment of a tripolar East Asia–Pacific (EAP) teleconnection pattern (also referred to as the Pacific–Japan wave train) along the East Asia coasts from tropics to high latitudes (Fig. 9c). EAP pattern is a dominant mode of variability in the summer atmospheric circulation, strongly influences climate variations around East Asia and the Northwestern Pacific, and yet hard to be captured faithfully in dynamic models (Nitta 1987; Li et al. 2012; Lin et al. 2018; Park et al. 2018). In the reduced skill years, the EAP appears as an anomalous positive–negative–positive alternating pattern in 500-hPa geopotential height and an anomalous anti-cyclone–cyclone–anticyclone pattern in 850-hPa wind field

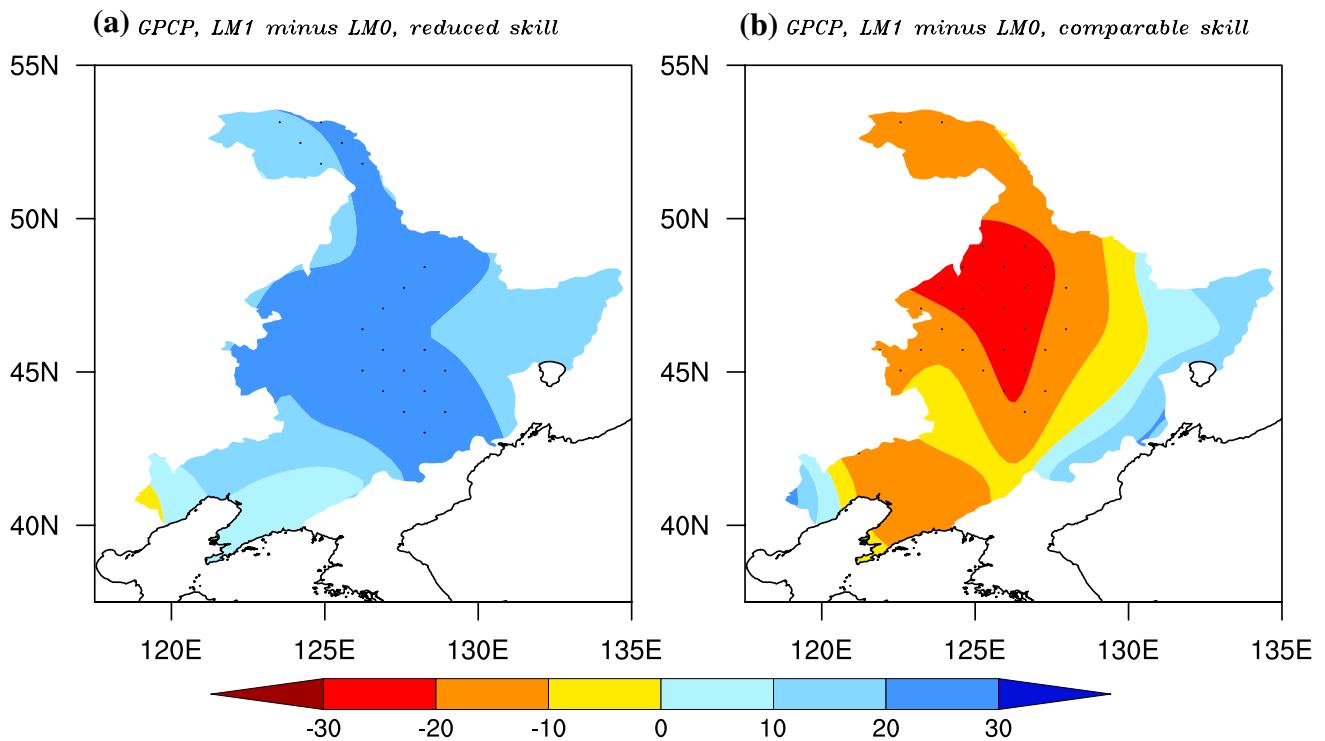


Fig. 8 Same as Fig. 6 but over Northeast China in August

approximately at 120°E between 20° N and 80° N (Fig. 9a), and vice versa in the comparable skill years (Fig. 9b).

At LM0, the model reproduces the EAP pattern in the reduced skill years and the positive geopotential height anomaly over Northeast China in the comparable skill years, although the positive anomaly west of the NWPSH is weaker than the observation in the reduced skill years (Fig. 9d, e). For LM1 in the reduced skill years, this EAP teleconnection pattern is absent and a negative-west versus positive-east dipole anomaly appears over the high latitudes instead (Fig. 9g). However, the positive geopotential height anomaly over Northeast China is still predicted in the comparable skill years at LM1 (Fig. 9h). The BCC_CSM1.1m model captures the differences of the EAP pattern between the reduced and comparable skill years at LM0 (Fig. 9f), such that the positive height anomaly over subtropical Northwest Pacific and the negative anomaly over Northeast China jointly provide moisture and cold air to Northeast China in reduced skill years, contributing to the formation of rainfall.

Earlier studies have revealed that summer rainfall over Northeast China is collectively affected by monsoon and synoptic-scale transients named Northeast China cold vortex (Lian et al. 2016; Sun et al. 2016; Fang et al. 2018). Here we construct composites for such transients in August based on the variance of the 2.5–6 day band-pass-filtered 500-hPa geopotential height of the ERA5 reanalysis. It is clear that in reduced skill years, cold vortex activities are elevated over

Northeast China giving rise to rainy Augusts (Fig. 10a, b). These synoptic transients likely originate around Novaya Zemlya, move southeastward with diminishing intensity, and re-strengthen near Lake Baikal and continuously moving eastward until arrive at Northeast China (Fig. 10c). During this process, the EAP teleconnection pattern plays a critical role as the large-scale steering flow for these transients. Therefore, the model's failure to predict EAP at LM1 in reduced skill years propagates to rainfall biases partly through the interaction between EAP and the activity of Northeast cold vortex.

5 Summary and discussions

In this study, the skills of S2S prediction of the EASM rainfall are evaluated using hindcast records from the BCC_CSM1.1m, the operational S2S model in China. Specifically, we made an attempt to identify and understand the factors responsible for the rapid decline of the prediction skill for summer rainfall from LM0 to LM1 over this domain.

The model exhibits considerable fidelity in capturing the climatological EASM rainfall, with the TCC prediction skill dropping rapidly from LM0 to LM1 and then fluctuating remarkably throughout LM2 to LM12. Skillful predictions of the EASM rainfall are seen over most domain at the shortest lead time (LM0, about 2 weeks) but become unskillful

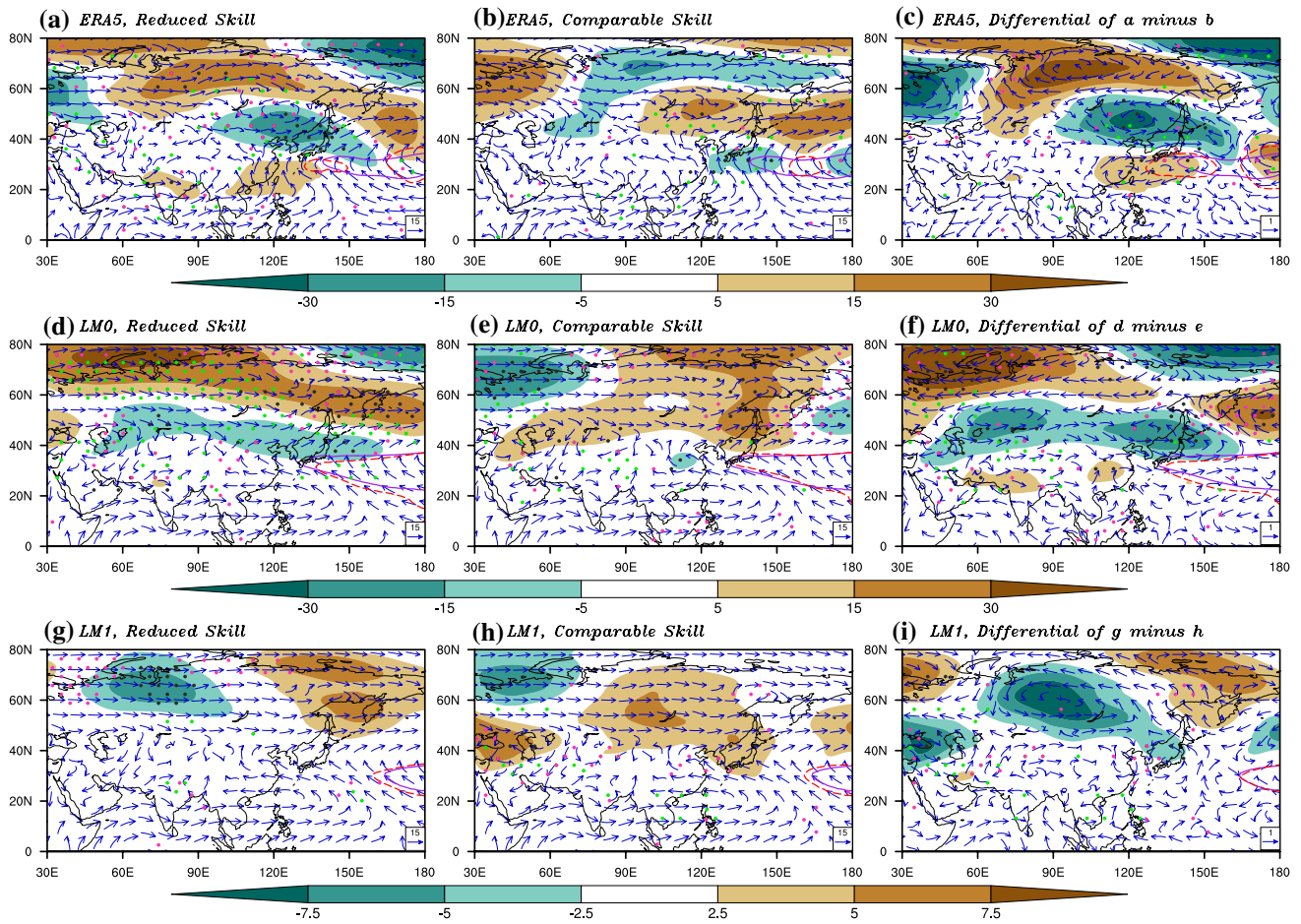


Fig. 9 Same as Fig. 7 but corresponding with Northeast China

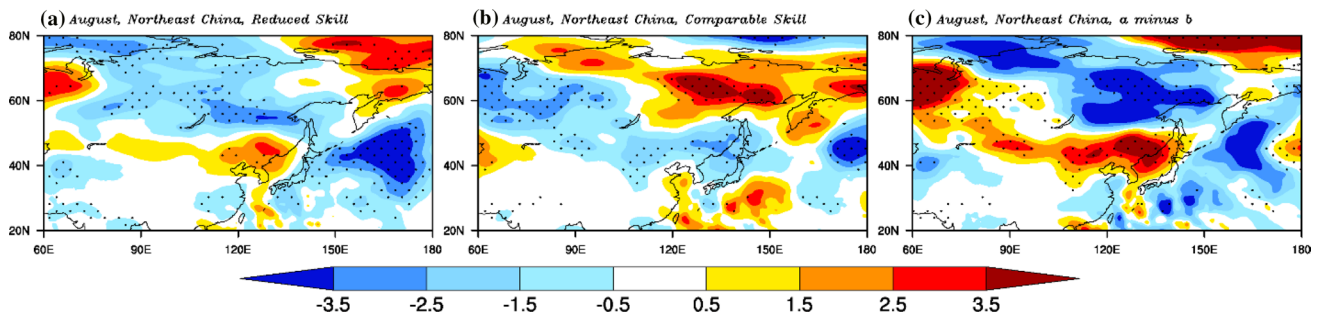


Fig. 10 Observational composite patterns of the synoptic-scale transients (dagpm) corresponding with Northeast China, constructed by the variance of the 2.5–6 day band-pass-filtered 500-hPa geopotential height; stipple areas represent the statistical significance at the 0.2 level

over the northeast China and the sparse central and southern Asia at LM1.

The dramatic decline of the EASM rainfall prediction skill from LM0 to LM1 is mainly associated with the inferior skills over Central China in July and Northeast China in August. Further composite analysis taking advantage of interannual variations of the S2S prediction

skills reveals the model’s difficulties in predicting above-normal precipitation over the eastern Central China and over Northeast China in the respective months and the associated extratropical large-scale circulation anomalies at longer lead time (i.e., LM1). For Central China in July, the reduced skill is tied to the model’s inability to capture the anomalous meridional displacement and intensity of

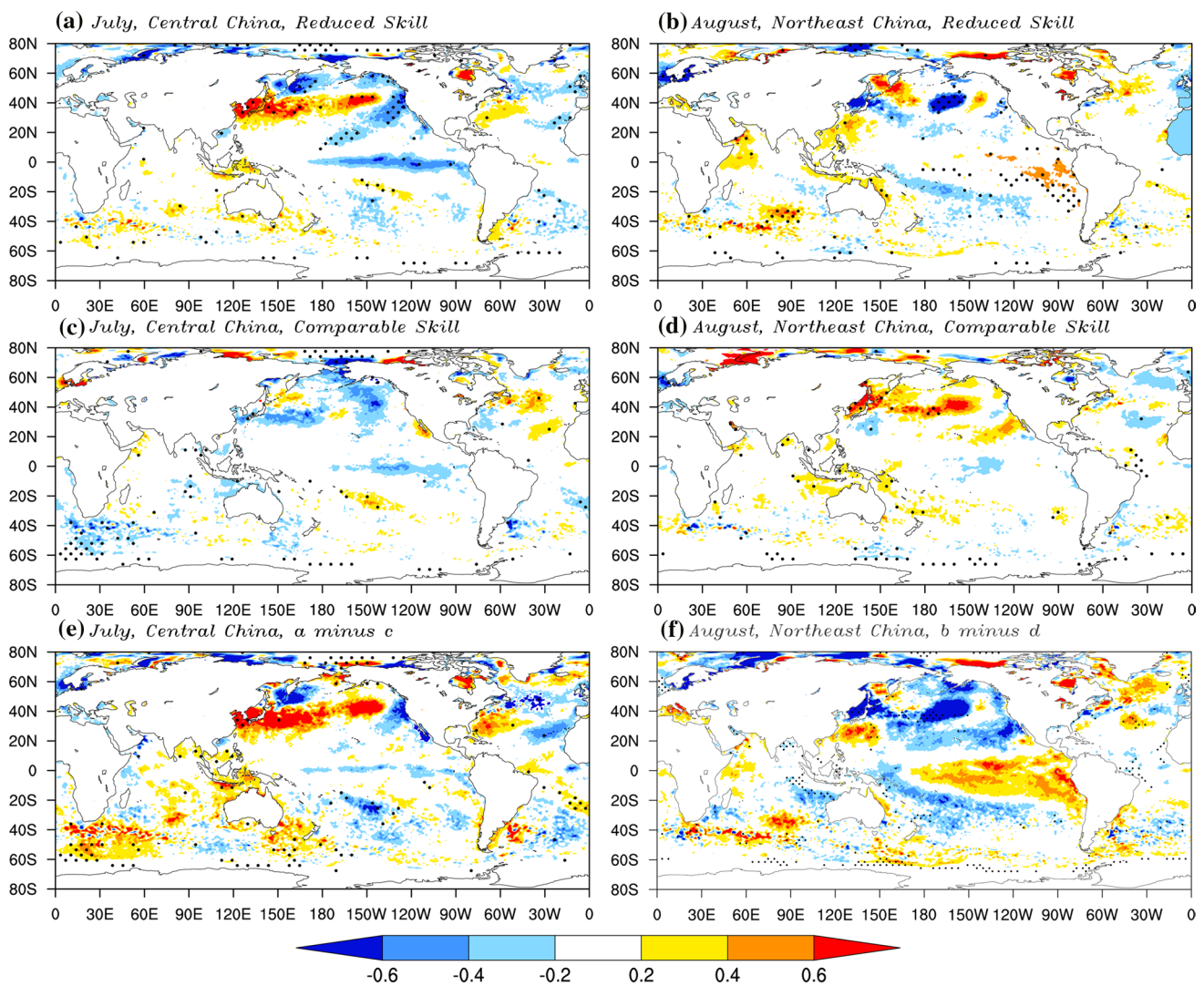


Fig. 11 Observational composite and difference patterns of the sea surface temperature anomaly ($^{\circ}\text{C}$) corresponding with Central China (**a**, **c**, **e**) and Northeast China (**b**, **d**, **f**); stipples represent the statistical significance at the 0.2 level

the NWPSH. For Northeast China in August, model fails to forecast the establishment of the EAP teleconnection pattern in one-month advance, which modulates moisture and cold air transport into Northeast China and steers synoptic transients to create rainfall in this region. The difficulties in predicting the large-scale circulation anomalies come from multiple factors. These include the spontaneous excitation of atmospheric teleconnection patterns (as internal modes of low-frequency variability), the model biases in faithfully reproducing the mean atmospheric state that supports the growth and decay of teleconnection patterns, the model deficiencies in capturing aspects of extratropical air-sea interactions, and finally, potential mis-representations of remote forcing such as those originated from the tropics and/or nearby monsoon regions (e.g., errors associated with the problems in simulating Indian monsoon

precipitation and thus the resulted thermal forcing (Son et al. 2021)).

Air-sea interaction is known to be an essential feature of interannual variability in the monsoon rainfall. Composites of sea surface temperature anomaly (SSTA) (Fig. 11) following the classification of reduced and comparable skill years offer a quick glimpse of the probable ocean footprints related to the atmosphere circulation anomalies discussed before. The difference of the SSTA composite corresponding to Central China shows significant positive anomaly over North Pacific at 40°N (Fig. 11e), a region also characterized by positive 500-hPa geopotential height anomaly and 850-hPa anticyclonic wind anomaly (Fig. 7c). The difference of the SSTA composite based on the Northeast China classification shows an anomalous positive–negative–positive tripolar pattern along the East Asia coasts (Fig. 11f), consistent

with the atmospheric circulation anomalies (Fig. 9c). Since downdraft, associated with the positive geopotential height and anticyclonic wind anomalies in lower-to-middle troposphere favors the formation of warm SSTA, the composite results suggest that SSTA seen here are likely forced by atmospheric circulation anomalies. These findings hint that the decline of subseasonal prediction skill of summer rainfall over East Asia from LM0 to LM1 may be largely attributed to model's inability to capture modes of atmospheric internal variability (including subtropical highs and EAP), not to model problems in simulating the correct temporal-spatial evolution of SST in adjacent ocean basins.

Results reported here have informed the skill of S2S prediction of the EASM rainfall by the BCC_CSM1.1m model, and specifically, revealed factors limiting such skills. The identification and understanding of these factors suggest that more skillful predictions could be expected with the continuous improvement of the dynamical models used; nonetheless, it is of equal importance to note that standing on the present prediction capability, the level of confidence we might place upon S2S predictions by dynamic models should be effectively be stratified by large-scale circulation anomalies known to significantly affect the prediction skill.

Acknowledgements This work is jointly supported by China National Key Research and Development Program on Monitoring, Early Warning and Prevention of Major Natural Disaster (2018YFC1506005), Forecaster Special Project of China Meteorological Administration (CMAYBY2020-071), Fund Project of Collaborative Innovation in Science and Technology in Bohai Sea Rim (QYXM201904) and the China Scholarship Council (award to Na Wang for 1 year's visit abroad at the Georgia Institute of Technology). Yi Deng is in part supported by the U.S. National Science Foundation (NSF) through Grant AGS-2032532 and by the U.S. National Oceanic and Atmospheric Administration (NOAA) through Grant NA20OAR4310380.

References

- Adler RF et al (2018) The global precipitation climatology project (GPCP) monthly analysis (new version 2.3) and a review of 2017 global precipitation. *Atmosphere* 9(4):138. <https://doi.org/10.3390/atmos9040138>
- Charney JG, Shukla J (1981) Predictability of monsoons chap 6. In: Lighthill J, Pearce RP (eds) *Monsoon dynamics*. Cambridge University Press. <https://doi.org/10.1017/CBO9780511897580.009>
- Cheng Y, Tang Y, Zhou X, Jackson P, Chen D (2010) Further analysis of singular vector and ENSO predictability in the Lamont model—part I: singular vector and the control factors. *Clim Dyn* 35:807–826. <https://doi.org/10.1007/s00382-009-0595-7>
- de Andrade FM, Coelho CAS, Cavalcanti IFA (2019) Global precipitation hindcast quality assessment of the subseasonal to seasonal (S2S) prediction project models. *Clim Dyn* 52:5451–5475. <https://doi.org/10.1007/s00382-018-4457-z>
- Dong B, Wilcox LJ, Highwood EJ, Sutton RT (2019) Impacts of recent decadal changes in Asian aerosols on the East Asian summer monsoon: roles of aerosol–radiation and aerosol–cloud interactions. *Clim Dyn* 53:3235–3256. <https://doi.org/10.1007/s00382-019-04698-0>
- Fang YH et al (2018) The remote responses of early summer cold vortex precipitation in Northeastern China compared with the previous sea surface temperatures. *Atmos Res* 214:399–409. <https://doi.org/10.1016/j.atmosres.2018.08.007>
- Griffies SM, Gnanadesikan A, Dixon KW, Dunne JP, Gerdes R, Harrison MJ, Rosati A, Russell JL, Samuels BL, Spelman MJ, Winton M, Zhang R (2005) Formulation of an ocean model for global climate simulations. *Ocean Sci* 1:45–79. <https://doi.org/10.5194/os-1-45-2005>
- Hersbach H et al (2020) The ERA5 global reanalysis. *Q J R Meteorol Soc* 146:1999–2049. <https://doi.org/10.1002/qj.3803>
- Ji J, Huang M, Li K (2008) Prediction of carbon exchange between China terrestrial ecosystem and atmosphere in 21st century. *Sci China Ser D Earth Sci* 51:885–898. <https://doi.org/10.1007/s11430-008-0039-y>
- Jie W, Vitart F, Wu T, Liu X (2017) Simulations of Asian Summer Monsoon in the Sub-seasonal to Seasonal Prediction Project (S2S) database: simulations of Asian summer monsoon in the S2S database. *Q J R Meteorol Soc* 143:2282–2295. <https://doi.org/10.1002/qj.3085>
- Johnson SJ et al (2019) SEAS5: the new ECMWF seasonal forecast system. *Geosci Model Dev* 12:1087–1117. <https://doi.org/10.5194/gmd-12-1087-2019>
- Keane RJ et al (2019) Fast biases in monsoon rainfall over Southern and Central India in the Met Office unified model. *J Clim* 32:6385–6402. <https://doi.org/10.1175/JCLI-D-18-0650.1>
- Kim HM, Webster PJ, Curry JA, Toma VE (2012) Asian summer monsoon prediction in ECMWF System 4 and NCEP CFSv2 retrospective seasonal forecasts. *Clim Dyn* 39:2975–2991. <https://doi.org/10.1007/s00382-012-1470-5>
- Kitoh A et al (2013) Monsoons in a changing world: a regional perspective in a global context. *J Geophys Res* 118:3053–3065. <https://doi.org/10.1002/jgrd.50258>
- Kug JS, Kang IS, Choi DH (2008) Seasonal climate predictability with tier-one and tier-two prediction systems. *Clim Dyn* 31:403–416. <https://doi.org/10.1007/s00382-007-0264-7>
- Li J, Zeng Q (2002) A unified monsoon index. *Geophys Res Lett*. <https://doi.org/10.1029/2001GL013874>
- Li J, Zeng Q (2003) A new monsoon index and the geographical distribution of the global monsoons. *Adv Atmos Sci* 20:299–302. <https://doi.org/10.1007/s00376-003-0016-5>
- Li J, Zeng Q (2005) A new monsoon index, its interannual variability and relation with monsoon precipitation. *Clim Environ Res* 10(3):351–365. <https://doi.org/10.3878/j.issn.1006-9585.2005.03.09> (In Chinese)
- Li CF, Lu RY, Dong BW (2012) Predictability of the western North Pacific summer climate demonstrated by the coupled models of ENSEMBLES. *Clim Dyn* 39:329–346. <https://doi.org/10.1007/s00382-011-1274-z>
- Li Y et al (2019) Multi-scale temporal-spatial variability of the East Asian summer monsoon frontal system: observation versus its representation in the GFDL HiRAM. *Clim Dyn* 52:6787–6798. <https://doi.org/10.1007/s00382-018-4546-z>
- Li J, Wang B, Yang YM (2020) Diagnostic metrics for evaluating model simulations of the East Asian Monsoon. *J Clim* 33:1777–1801. <https://doi.org/10.1175/JCLI-D-18-0808.1>
- Lian Y, Shen B, Li S, Liu G, Yang X (2016) Mechanisms for the formation of Northeast China cold vortex and its activities and impacts: an overview. *J Meteorol Res* 30:881–896. <https://doi.org/10.1007/s13351-016-6003-4>
- Lin X, Li C, Lu R, Scaife AA (2018) Predictable and unpredictable components of the summer East Asia-Pacific teleconnection

- pattern. *Adv Atmos Sci* 35:1372–1380. <https://doi.org/10.1007/s00376-018-7305-5>
- Liu Y, Ren HL (2015) A hybrid statistical downscaling model for prediction of winter precipitation in China. *Int J Climatol* 35(7):1309–1321. <https://doi.org/10.1002/joc.4058>
- Liu Y, Ren HL (2017) Improving ENSO prediction in CFSv2 with an analogue-based correction method. *Int J Climatol* 37:5035–5046. <https://doi.org/10.1002/joc.5142>
- Liu X et al (2014) Subseasonal forecast skills and biases of global summer monsoons in the NCEP climate forecast system version 2. *Clim Dyn* 42:1487–1508. <https://doi.org/10.1007/s00382-013-1831-8>
- Liu X et al (2015) Performance of the seasonal forecasting of the Asian summer monsoon by BCC_CSM1.1(m). *Adv Atmos Sci* 32:1156–1172. <https://doi.org/10.1007/s00376-015-4194-8>
- Liu Y, Ren HL, Scaife AA, Li CF (2018) Evaluation and statistical downscaling of East Asian summer monsoon forecasting in BCC and MOHC seasonal prediction systems. *Q J R Meteorol Soc* 144(717):2798–2811. <https://doi.org/10.1002/qj.3405>
- Liu Y et al (2021) An operational statistical downscaling prediction model of the winter monthly temperature over China based on a multi-model ensemble. *Atmos Res* 249:105262. <https://doi.org/10.1016/j.atmosres.2020.105262>
- Ma JH, Wang HJ (2014) Design and testing of a global climate prediction system based on a coupled climate model. *Sci China Earth Sci* 57:2417–2427. <https://doi.org/10.1007/s11430-014-4875-7>
- Nitta T (1987) Convective activities in the tropical western Pacific and their impact on the northern hemisphere summer circulation. *J Meteorol Soc Jpn* 65:373–390. https://doi.org/10.2151/jmsj1965.65.3_373
- Park HJ, Kryjov VN, Ahn JB (2018) One-month-lead predictability of Asian summer monsoon indices based on the zonal winds by the APCC multimodel ensemble. *J Clim* 31:8945–8960. <https://doi.org/10.1175/JCLI-D-17-0816.1>
- Ramage CS (1971) Monsoon meteorology vol 15. In: Miller DH (ed) *International geophysics*. Academic Press
- Ren HL et al (2017) Prediction of primary climate variability modes at the Beijing Climate Center. *J Meteorol Res* 31:204–223. <https://doi.org/10.1007/s13351-017-6097-3>
- Saha S et al (2014) The NCEP climate forecast system version 2. *J Clim* 27:2185–2208. <https://doi.org/10.1175/JCLI-D-12-00823.1>
- Shukla J (1998) Predictability in the midst of chaos: a scientific basis for climate forecasting. *Science* 282:728–731. <https://doi.org/10.1126/science.282.5389.728>
- Singh B, Cash B, Kinter JL III (2019) Indian summer monsoon variability forecasts in the North American multimodel ensemble. *Clim Dyn* 53:7321–7334. <https://doi.org/10.1007/s00382-018-4203-6>
- Son J-H, Seo K-H, Wang B (2019) Dynamical control of the Tibetan Plateau on the East Asian Summer Monsoon. *Geophys Res Lett* 46(13):7672–7679. <https://doi.org/10.1029/2019GL083104>
- Son J-H, Seo K-H, Wang B (2020) How does the Tibetan Plateau dynamically affect downstream monsoon precipitation? *Geophys Res Lett* 47(23):e2020GL090543. <https://doi.org/10.1029/2020GL090543>
- Son J-H, Seo K-H, Son S-W, Cha D-H (2021) How does Indian Monsoon regulate the northern hemisphere stationary wave pattern? *Front Earth Sci* 8:599745. <https://doi.org/10.3389/feart.2020.599745>
- Sun ZB, Cao R, Ni DH (2016) A classification of summer precipitation patterns over Northeast China and their atmospheric circulation characteristics. *Trans Atmos Sci* 39(1):18–27. <https://doi.org/10.13878/j.cnki.dqkxxb.20140415001> (In Chinese)
- Trenberth KE, Stepaniak DP, Caron JM (2000) The Global monsoon as seen through the divergent atmospheric circulation. *J Clim* 13:3969–3993. [https://doi.org/10.1175/1520-0442\(2000\)013%3c3969:TGMAST%3e2.0.CO;2](https://doi.org/10.1175/1520-0442(2000)013%3c3969:TGMAST%3e2.0.CO;2)
- Tzeng RY, Lee YH (2001) The effects of land–surface characteristics on the East Asian summer monsoon. *Clim Dyn* 17:317–326. <https://doi.org/10.1007/s003820000115>
- Vitart F, Robertson AW (2018) The sub-seasonal to seasonal prediction project (S2S) and the prediction of extreme events. *Npj Clim Atmos Sci* 1:3. <https://doi.org/10.1038/s41612-018-0013-0>
- Wang B, Ding Q (2006) Changes in global monsoon precipitation over the past 56 years. *Geophys Res Lett* 33:L06711. <https://doi.org/10.1029/2005GL025347>
- Wang B, Ho L (2002) Rainy season of the Asian-Pacific summer monsoon. *J Clim* 15:386–398. [https://doi.org/10.1175/1520-0442\(2002\)015%3c0386:RSOTAP%3e2.0.CO;2](https://doi.org/10.1175/1520-0442(2002)015%3c0386:RSOTAP%3e2.0.CO;2)
- Wang B et al (2008) How to measure the strength of the East Asian summer monsoon. *J Clim* 21:4449–4463. <https://doi.org/10.1175/2008JCLI2183.1>
- Wang B, Jin C, Liu J (2020a) Understanding future change of global monsoons projected by CMIP6 models. *J Clim* 33:6471–6489. <https://doi.org/10.1175/JCLI-D-19-0993.1>
- Wang L, Ren HL, Zhu J, Huang B (2020b) Improving prediction of two ENSO types using a multi-model ensemble based on stepwise pattern projection model. *Clim Dyn* 54:3229–3243. <https://doi.org/10.1007/s00382-020-05160-2>
- Wang Y et al (2020c) Multi-model ensemble sub-seasonal forecasting of precipitation over the maritime continent in boreal summer. *Atmosphere* 11:515. <https://doi.org/10.3390/atmos11050515>
- Winton M (2000) A reformulated three-layer sea ice model. *J Atmos Oceanic Technol* 17:525–531. [https://doi.org/10.1175/1520-0426\(2000\)017%3c0525:ARTLSI%3e2.0.CO;2](https://doi.org/10.1175/1520-0426(2000)017%3c0525:ARTLSI%3e2.0.CO;2)
- Wu TW et al (2010) The Beijing Climate Center atmospheric general circulation model: description and its performance for the present-day climate. *Clim Dyn* 34:123–147. <https://doi.org/10.1007/s00382-008-0487-2>
- Wu TW et al (2014) An overview of BCC climate system model development and application for climate change studies. *J Meteorol Res* 28(1):34–56. <https://doi.org/10.1007/s13351-014-3041-7>
- Zhou F et al (2020) Seasonal predictability of primary East-Asian summer circulation patterns by three operational climate prediction models. *Q J R Meteorol Soc* 146:629–646. <https://doi.org/10.1002/qj.3697>

Publisher's Note Springer Nature remains neutral with regard to jurisdictional claims in published maps and institutional affiliations.